RSC Advances

ROYAL SOCIETY OF CHEMISTRY

www.rsc.org/advances

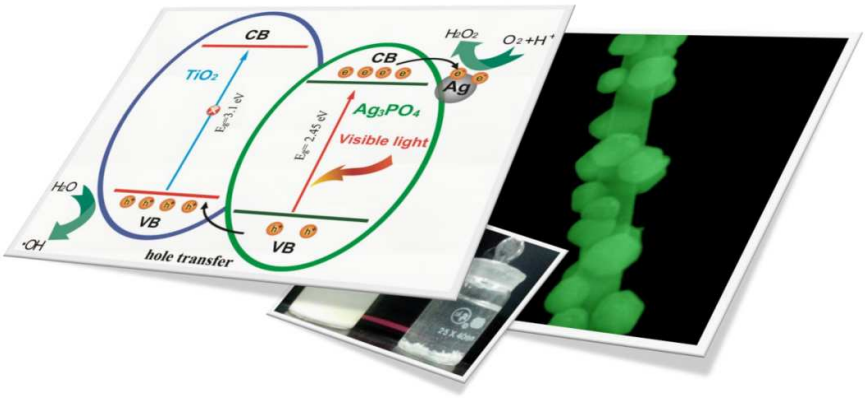

One-dimensional Ag_3PO_4/TiO_2 heterostructure exhibits enhanced photocatalytic activity due to good visible light absorption capability and excellent charge separation characteristics of the formed heterojunction.

Cite this: DOI: 10.1039/c0xx00000x

www.rsc.org/xxxxxx

ARTICLE TYPE

One-dimensional Ag_3PO_4/TiO_2 heterostructure with enhanced photocatalytic activity for the degradation of 4-nitrophenol

Mingyi Zhang, Lu Li and Xitian Zhang*

Received (in XXX, XXX) Xth XXXXXXXXX 20XX, Accepted Xth XXXXXXXXX 20XX
DOI: 10.1039/b000000x

One-dimensional TiO_2 nanofibers were synthesized by an electrospinning method. Subsequently, Ag_3PO_4/TiO_2 heterostructure were successfully fabricated through a simple deposition–precipitation reaction. The Ag_3PO_4/TiO_2 heterostructures exhibited enhanced photocatalytic performance under visible light. The improved photocatalytic activities are attributed to the visible light absorption enhanced by Ag_3PO_4 and the formation of a heterojunction between TiO_2 and Ag_3PO_4, which can effectively accelerate the charge separation and transfer. The heterostructures can be reclaimed easily by sedimentation without a decrease of the photocatalytic activity due to the large length to diameter ratio of nanofiber framework.

1. Introduction

The applications on solar energy conversion and degradation of pollution by semiconductor photocatalysts have received extensive attention in modern society[1-3]. Considering utilizing the solar energy more effectively, the development of efficient visible-light-driven (VLD) photocatalysts has attracted worldwide attentions[4-18]. Recently, a new type of VLD photocatalyst, Ag_3PO_4, demonstrated by *Ye et al*[19] exhibited high photooxidative capabilities for O_2 evolution from water as well as organic dye decomposition under visible light irradiation. To further enhance its photochemical reactivity and stability, many studies have been focused on constructing the Ag_3PO_4-base composite photocatalyst with different materials[20-24]. Up to now, the Ag_3PO_4-base composite materials mainly divided into two kinds, zero dimensional nanoparticles and two dimensional films[25-28]. Among these materials, zero dimensional Ag_3PO_4-base composite nanoparticles exhibited a high photocatalytic activity due to its high surface area. However, the suspended particulate catalysts are easily lost in the process of photocatalytic reaction and separation, which may repollute the treated water again. Meanwhile, the two dimensional Ag_3PO_4-base nanofilms can be fixed and reclaimed easily, but the immobilization of nanofilms dramatically reduces the interfacial contact between photocatalysts and pollutants, resulting in lower photocatalytic efficiency. Therefore, it is a great interest to design efficient and practical Ag_3PO_4 photocatalysts with excellent photocatalytic characteristics and favorable recycling capability.

With a great potential to overcome these drawbacks, the one-dimensional electrospun nanofibers might be promising support for immobilization of nanostructured photocatalysts. Compared with the corresponding nanoparticles and thin films of Ag_3PO_4-base, the effects of the one-dimensional composite nanomaterials on the photocatalytic properties of Ag_3PO_4 have been rarely studied[29,30]. More specifically, the use of one-dimensional electrospun nanofibers as co-photocatalysts is attracting increasing attention in the fields of photochemistry and photocatalysis. For example, our group reported that $Bi_4Ti_3O_{12}$ composites showed rapid sedimentation over a time scale of minutes, which can also be useful for the gravity separation of these particles in photocatalytic applications[9]. Furthermore, in contrast to one individual semiconductor photocatalyst, hybrid one-dimensional photocatalysts integrate the synergistic effects of the individual species, which can endow the composite systems with prolonged lifetime of carriers, enhanced catalytic performance as well as higher chemical stability.

Based on the above considerations, in this work we report a successful attempt for the fabrication of the Ag_3PO_4/TiO_2 heterostructures *via* a simple electrospinning technique and deposition–precipitation method. The as-prepared Ag_3PO_4/TiO_2 heterostructures has an interesting structure with uniform size consisting of a TiO_2 nanofiber core and a nanocubes-based Ag_3PO_4 shell. The special hierarchical structure, high light-harvesting capacity and the nanoscale heterostructure make it be an excellent candidate for the degradation of pollution with enhanced photocatalytic efficiency.

2. Experimental

2.1. Preparation of TiO_2 Nanofibers

Firstly, 2 g Poly(vinyl pyrrolidone) powder (PVP, Mw = 1 300 000) was added to a mixture of 9 mL absolute ethanol and 5mL acetic acid in a capped bottle. The obtained solution was stirred for 1 h to generate a homogeneous solution. Then 2.0 g $Ti(OC_4H_9)_4$ was added to the solution, the mixture was

continuously stirred for another 1 h to make precursor solution. 3 mL of the precursor solution was placed in a 5 mL syringe equipped with a blunt metal needle of 0.8 mm outer diameter and 0.6 mm inner diameter. A stainless steel plate covered with a sheet of aluminum foil was employed as the collector. The distance between the needle tip and collector was 15 cm, and the voltage was set at 9 kV. The as-collected nanofibers were calcined at 550 ℃ for 2 h to form anatase TiO_2 nanofibers.

2.2. Fabrication of Ag_3PO_4/TiO_2 hierarchical nanostructures

Then, Ag_3PO_4/TiO_2 composites were prepared by deposition–precipitation and photoreduction process. Briefly, 50 mg TiO_2 nanofibers was added to 100 mL of distilled water, and the suspension was stirred magnetically for 30 min. Then, 50 mL $AgNO_3$ aqueous solution (15mM) was added into the suspension and stirred for another 30 min. After that, a certain amount of $NH_3 \cdot H_2O$ (2 wt.% NH_3) was added to make sure that Ag^+ reacts with NH_3. Finally, 50 mL of $Na_2HPO_4 \cdot 12H_2O$ aqueous solution (5mM) was added dropwise into the suspension, and stirred for 120 min. All the above processes were carried out at ambient temperature. The products were filtered, washed by deionized water, and then dried at 70 ℃ for 2 h. For comparison, Ag_3PO_4 samples were also prepared by a similar process in the absence of TiO_2 nanofibers.

2.3 Characterization

The morphology of the samples was observed by a field emission scanning electron microscope (FE–SEM; SU–70, Hitachi, Japan) equipped with energy dispersive X–ray (EDX) spectrometer. The crystalline structures of the samples were characterized by X–ray powder diffraction (XRD, D/max2600, Rigaku, Japan) and transmission electron microscopy (TEM; FEI, Tecnai TF20). UV–vis diffuse reflectance spectra (DRS) of the samples were obtained by using a UV–vis spectrometer (Perkin–Elmer, Lambda 850).

The photocurrent were conducted by using an electrochemical analyzer (CHI660E, Shanghai, China) with a standard three–electrode configuration, which employed a Pt wire as a counter electrode, a saturated calomel electrode as a reference electrode and fluorine–doped tin oxide (FTO) as working electrode. 10 mg of sample powder was dispersed into 2 mL of N, N–dimethylflormamide under ultrasonication for 10 min to obtain slurries. The as–prepared slurries were spread onto the surface of FTO glasses to obtain sample films with the region of 1×1 cm. These as–prepared FTO glasses electrodes were dried at 100 ℃ for 60 minutes under ambient conditions to improve adhesion. The 50mL 0.5M Na_2SO_4 (pH = 6.8) was used as the electrolyte solution. A 300 W xenon lamp with a 420 nm cut–off filter was employed as a visible light photosource.

2.4 Photocatalytic Test.

The degradation of 4-nitrophenol (4-NP) was carried out in a 200 mL beaker containing 100 mL 4-NP with a concentration of 1×10^{-5} mol/L and 50 mg of the as–prepared photocatalysts with vigorous magnetic stirring at room temperature. A 300 W xenon lamp with a 420 nm cut–off filter was employed as a visible light photosource. The solution was stirred in the dark for 30 min to obtain a good dispersion and reach adsorption–desorption equilibrium between the 4-NP molecules and the catalyst surface. The concentration of 4-NP was measured by UV–visible spectrophotometer at given intervals during the degradation process of 4-NP.

3. Results and discussion

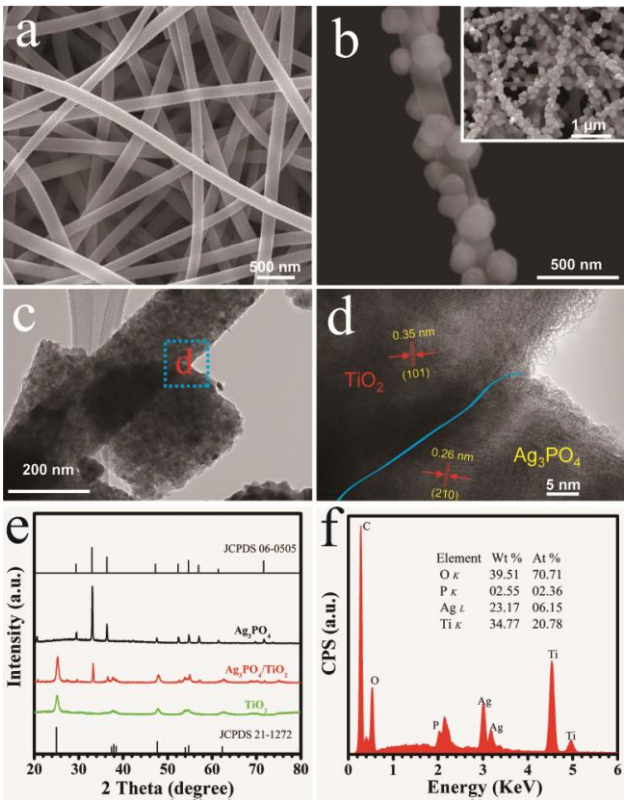

Fig.1 (a) SEM images of TiO_2 nanofibers. (b) SEM images of Ag_3PO_4/TiO_2 heterostructures. (c) TEM images of Ag_3PO_4/TiO_2 heterostructures. (d) HRTEM images of Ag_3PO_4/TiO_2 heterostructures. (e) XRD patterns of the samples. (f) EDX patterns of the samples.

The morphology, crystallinity and composition of the products were characterized by SEM, TEM, XRD and EDX. Fig. 1a shows an SEM image of the pure TiO_2 nanofibers which were fabricated by electrospinning followed by calcination at 550 ℃ for 2 h. It can be clearly seen that the TiO_2 nanofibers are of a relatively smooth surface without secondary structures and their diameters are 200 nm. However, after being subjected to the solution of Ag^+ and PO_4^{3-}, Ag_3PO_4 nanostructures grew on the surface of TiO_2 nanofibers after deposition–precipitation process. Fig. 1b shows the SEM images of the Ag_3PO_4/TiO_2 heterostructures. As observed inset of Fig. 1b, Ag_3PO_4 nanocubes grow on the surface of TiO_2 nanofibers after deposition–precipitation reaction. It can be seen from the high magnification SEM image of Ag_3PO_4/TiO_2 heterostructures that the diameters of Ag_3PO_4 nanocubes are about 50-150 nm. Close inspection at the junction of TiO_2 nanofibers and Ag_3PO_4 nanocubes shows that the Ag_3PO_4 secondary structures have their roots inside the TiO_2 nanofibers, suggesting that the Ag_3PO_4 nanocubes is not just loosely attached to the TiO_2 nanofibers surface. Fig. 1c shows the typical TEM images of Ag_3PO_4/TiO_2 heterostructures. The TEM images reveal that Ag_3PO_4 secondary structures are coated around the primary

TiO_2 nanofibers substrates, coinciding with the results from the above SEM observations. The HRTEM image from Ag_3PO_4/TiO_2 heterostructures displays two types of clear lattice fringes as shown in Fig. 1d, respectively. The interplanar distance between the adjacent lattice fringes is 0.35 nm, which agreed well with the (101) plane of the anatase TiO_2. Another set of fringes for the interplanar distance of 0.26 nm correspond to the (210) lattice plane of Ag_3PO_4. The HRTEM image further exhibits the formation of heterostructures.

The XRD pattern (Fig. 1e) shows the crystallinity and phase purity of the Ag_3PO_4, TiO_2 nanofibers and Ag_3PO_4/TiO_2 heterostructures. The diffraction peaks of TiO_2 nanofibers are indexed to the pure anatase TiO_2 (JCPDS No. 21-1272) and those of Ag_3PO_4 powders are coincident with the cubic structure of Ag_3PO_4 (JCPDS No. 06-0505). No peaks of impurities can be observed, demonstrating the high phase purity of the as-prepared Ag_3PO_4 powders and TiO_2 nanofibers. Comparison with the Ag_3PO_4 powders and TiO_2 nanofibers, the Ag_3PO_4/TiO_2 heterostructures is well crystallized and all the diffraction peaks can well be indexed to the anatase TiO_2 and cubic structure of Ag_3PO_4, respectively. No feature peaks for impurities, such as Ag_2O are observed, indicating that Ag_3PO_4/TiO_2 heterostructures are successfully achieved by the deposition–precipitation reaction. Additionally, EDX spectrum of Ag_3PO_4/TiO_2 heterostructures was measured to determine the chemical composition of the heterostructures. The analysis results show that the atomic ratio of Ag to Ti is about 3 : 10 (Fig. 1f).

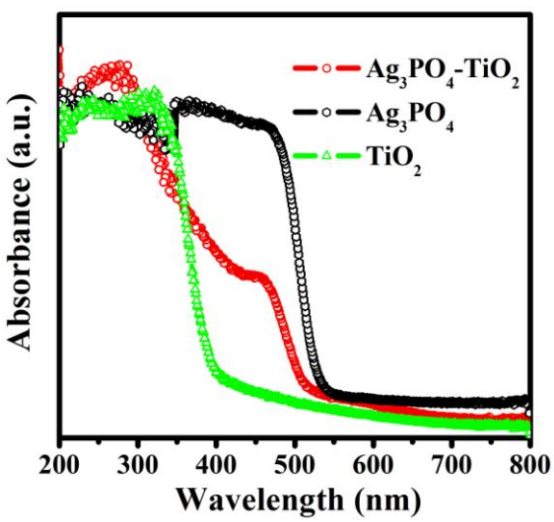

Fig.2 UV–vis diffuse reflectance spectre of samples.

The UV-Vis diffuse reflectance spectra of the pure TiO_2 nanofibers, Ag_3PO_4 powders and Ag_3PO_4/TiO_2 heterostructures are shown in Fig. 2. As observed in Fig. 2, the diffuse reflectance spectrum of TiO_2 nanofibers only exhibits the fundamental absorption band in the UV region, there are no more absorption in visible wavelengths. The UV-Vis spectrum of the Ag_3PO_4 sample indicates that it absorbs sunlight with a wavelength less than 510 nm, corresponding to 2.45 eV of band gap energy. However, for the Ag_3PO_4/TiO_2 heterostructures, except for the absorption band edge (370 nm) in the UV light range, a feature band edge of Ag_3PO_4 appears in the visible light range based on its UV-Vis spectrum. This feature of visible light absorption properties of the prepared Ag_3PO_4/TiO_2 photocatalyst can be attributed to the small band gap and large absorption coefficient of Ag_3PO_4. Taking into account the efficient use of visible light in a large part of the solar spectrum, we believe that the Ag_3PO_4/TiO_2 heterostructures with its long wavelength absorption band is an attractive photocatalyst for pollutant degradation.

To investigate the photocatalytic properties of the as-prepared photocatalyst, we also chose the 4-nitrophenol (4-NP) to evaluate the photocatalytic activity as it is more difficult to be degraded than the dyes in aqueous media. It is well-known 4-NP solution exhibits a strong absorption peak at 317 nm in neutral or acidic condition. Temporal changes in the concentration of 4-NP, as monitored by the maximal absorption of 4-NP in the UV–vis spectra over the as–prepared photocatalysts, are shown in Fig. 3a. The degradation efficiency of all the samples is defined as C/C_0, where C and C_0 represent the remnant and initial concentration of 4-NP, respectively. TiO_2 nanofibers, Ag_3PO_4 powders and Degussa-P25 are used as the photocatalytic reference. As shown in Fig. 3a, after visible light irradiation for 50 min, the TiO_2 nanofibers and Degussa-P25 had no photocatalytic activity under the visible light, except adsorption for 4-NP. Meanwhile, the degradation efficiency of 4-NP are about 70 and 99% for the Ag_3PO_4 powders and Ag_3PO_4/TiO_2 heterostructures, respectively. Obviously, the Ag_3PO_4/TiO_2 heterostructures exhibit enhanced photocatalytic activities for the degradation than TiO_2 nanofibers and Ag_3PO_4 powders. The enhanced photocatalytic activity can be attributed to the epitaxial growth of Ag_3PO_4 nanocubes on the surfaces of TiO_2 nanofibers and strong visible light absorptivity.

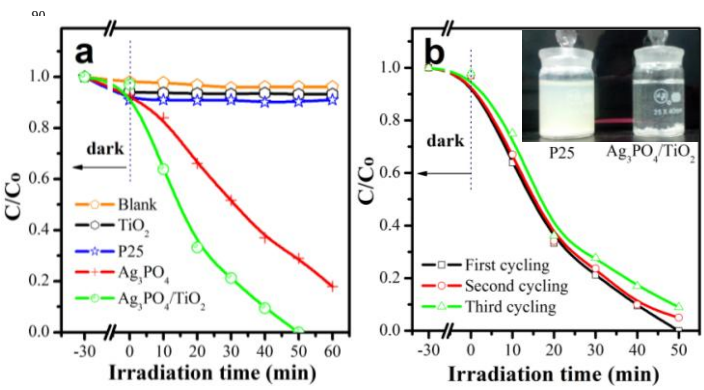

Fig. 3 (a) The comparisons of photocatalytic activities among the samples. (b) Degradation curves of 4-NP over Ag_3PO_4/TiO_2 heterostructures for reusing 3 times (Inset: Photographs of 4-NP solution which undergo visible light photo-degradation for 50 min with P25 and Ag_3PO_4/TiO_2 heterostructures and after sedimentation for 30 min).

The enhanced photocatalytic performance of Ag_3PO_4/TiO_2 is due to the following factors: On the one hand, according to DRS analysis, Ag_3PO_4/TiO_2 heterostructure exhibits enhanced absorption in visible light region. It is evident from the results that Ag_3PO_4/TiO_2 heterostructure absorbed more visible light

than pure TiO_2 and thus displayed better photocatalytic activity. On the other hand, the formed junction between Ag_3PO_4 and TiO_2 in the heterostructured photocatalysts can further prevent the recombination between photoelectrons and holes. In this work, the as-adopted fabrication route is successful to realize a close contact of Ag_3PO_4 with TiO_2 nanoparticles in Ag_3PO_4/TiO_2 heterostructure, as evidenced by SEM and TEM observation. Such close contact is more effective in suppression of the electron-hole recombination. The migration of photogenerated carriers was promoted because less of a barrier exists between Ag_3PO_4/TiO_2 heterostructure.

To confirm the stability of the high photocatalytic performance of the Ag_3PO_4/TiO_2 photocatalysts, the circulating runs in the photodegradation of 4-NP under visible light ($\lambda > 420$ nm) were checked. As shown in Fig. 3b, each experiment was carried out under identical conditions and, after three cycles, the photocatalytic activity of the Ag_3PO_4/TiO_2 heterostructures remained almost unchanged, clearly indicating the stability. Fig. S1 shows the XRD patterns and SEM images of Ag_3PO_4/TiO_2 catalyst after the catalytic reaction. After three catalytic runs, the position and the ratio of peaks are nearly the same to that of fresh photocatalyst. And, the secondary Ag_3PO_4 nanostructures are still very complete, clearly indicating the stability. Moreover, the photograph in Fig. 3b shows that the samples can be easily separated from the solution by sedimentation after 30 min, probably due to the large length to diameter ratio of the one-dimensional nanofibrous Ag_3PO_4/TiO_2 heterostructures. In comparison, the Degussa-P25 nanoparticles are still suspended after 30 minutes of precipitation in aqueous solution. It indicates that Ag_3PO_4/TiO_2 nanostructures display an efficient photoactivity for the degradation of organic pollutants under visible light irradiation and could easily be separated for reuse.

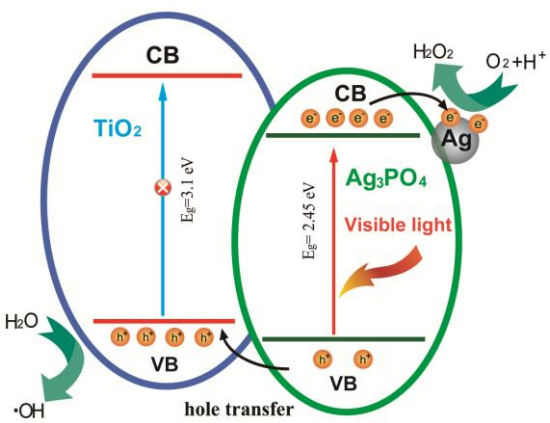

Scheme 1. Schematic of the band structures of Ag_3PO_4/TiO_2 heterostructures and possible electron–hole separations.

Scheme 1 illustrates a plausible mechanism for the photodegradation of 4-NP over Ag_3PO_4/TiO_2 heterostructures. As shown in Scheme 1, Ag_3PO_4 with narrow band gap energy (2.45 eV in this work) can be easily excited by visible light ($\lambda > 420$ nm, energy less than 2.95 eV) and induce the generation of photoelectrons and holes. In the case of TiO_2, it can not be excited by the visible-light irradiation with energy less than 2.95 eV due to its wide energy gap of about 3.11 eV in this work. Potentials of both conduction band and valence band of TiO_2 are more negative than those of Ag_3PO_4, photons generated holes in an Ag_3PO_4 particle quickly transfer to a TiO_2 particle, whereas photons generated electrons migrate to the surface of an Ag_3PO_4 particle. In such a way, the photoinduced electron–hole pairs can be effectively separated. The separation of electrons (in Ag_3PO_4) and holes (trapped in TiO_2) prevents the charge recombination, leading to higher photocatalytic activity of Ag_3PO_4. During the photocatalytic process, Ag^0 nanoparticles are produced by the partial reduction of Ag_3PO_4 by the photogenerated electrons (Fig. S2). The resultant Ag metals can trap the photo-generated electrons and thus inhibit the further decomposition of Ag_3PO_4[31,32]. Therefore, the formed $Ag/Ag_3PO_4/TiO_2$ interfaces can effectively promote charge separation and enhance the photocatalytic activity of the catalyst. The better separation of electrons and holes in the Ag_3PO_4/TiO_2 heterostructures is confirmed by the transient photocurrent responses (Fig. 4). In comparison with pure Ag_3PO_4, Ag_3PO_4/TiO_2 heterostructures exhibit an increased current density, about 3.5 times than that of the bare Ag_3PO_4. The increased current density indicates enhancing separation efficiency of photoinduced electrons and holes, which could be attributed to the heterojunctions between Ag_3PO_4 and TiO_2 and the electron trapping role of Ag nanoparticles.Mover, the photoluminescence emission spectra of the prepared the TiO_2 nanofibers and Ag_3PO_4/TiO_2 heterostructures also are consistent with the above results (Fig. S3).

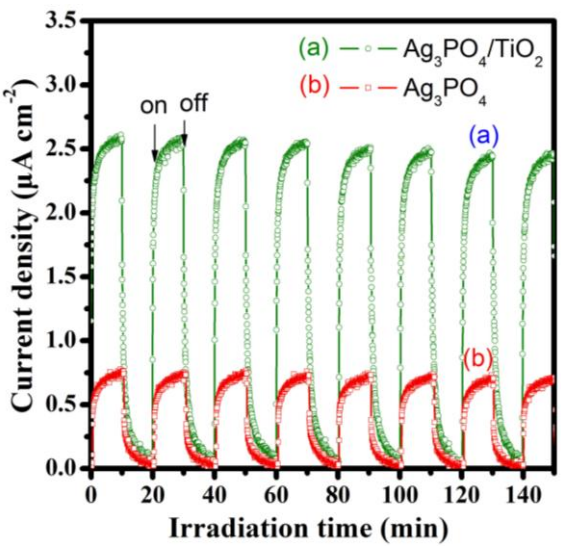

Fig. 4 Transient photocurrent response of the Ag_3PO_4 and Ag_3PO_4/TiO_2 heterostructures under visible light irradiation.

4. Conclusion

In summary, by using deposition–precipitation reaction and electrospinning technology, the Ag_3PO_4/TiO_2 heterostructures were successfully fabricated. In comparison to TiO_2 and Ag_3PO_4 samples, the Ag_3PO_4/TiO_2 heterostructures exhibits a high photocatalytic behavior for the decomposition of 4-NP, benefiting

from the heterojunction reducing the recombination of photogenerated electrons and holes by the photoinduced potential difference generated at the Ag_3PO_4/TiO_2 heterojunction interface. These results indicated that the Ag_3PO_4/TiO_2 heterostructures are promising candidate materials for wastewater treatment.

5. Acknowledgements

This work was partially supported by the Natural Science Foundation of China (no. 51172058, 51472066 and 51402076), the Natural Science Foundation of Heilongjiang Province (ZD201112 and QC2014C056) and Institution of Higher Education Doctoral Fund Jointly Funded Project (20112329110001) and Graduate Students' Scientific Research Innovation Project of Harbin Normal University (HSDSSCX2014－06).

Notes and references

Key Laboratory for Photonic and Electronic Bandgap Materials, Ministry of Education, School of Physics and Electronic Engineering, Harbin Normal University, Harbin 150025, P. R. China.
E-mail: xtzhangzhang@hotmail.com

References

1. A. Fujishma and K. Honda, *Nature*, 1972, **238**, 37−38.
2. A. F. Alkaim, Tarek A. Kandiel, F. H. Hussein, R. Dillert and D. W. Bahnemann, *Catal. Sci. Technol*., 2013, **3**, 3216–3222.
3. Y. Chen, M. D. Regulacio, S. H. Lim, Q. H. Xu, M. Y. Han, *Chem.–Eur. J.*, 2012, **18**, 11258−11263.
4. P. Wang, B. Huang, Q. Zang, X. Zang, X. Qin, Y. Dai, J. Zang, J. Yu, H. Liu, Z. Lou, *Chem.–Eur. J.* , 2010, **16**, 10042−10047.
5. C. An, S. Peng, Y. Sun, *Adv. Mater.* , 2010, **22**, 2570−2574.
6. H. Wang, J. Gao, T. Q. Guo, R. M. Wang, L. Guo, Y. Liu and J. H. Li, *Chem. Commun.* , 2012, **48**, 275−277.
7. Z. Q. Liu, X. H. Xie, Q. Z. Xu, S. H. Guo, N. Li, Y. B. Chen, Y. Z. Su. Electrochim. Acta, 2013, **98**, 268-273.
8. H. Wang, J. T. Yang, X. L. Li, H. Z. Zhang, J. H. Li, L. Guo, *Small* , 2012, **8**, 2802−2806.
9. Y. Liu, M. Y. Zhang, L. Li, X. T. Zhang, *Appl. Catal. B:Environ.*, 2014，160–161，757–766
10. H. Wang, L. He, L. H. Wang, P. F. Hu, L. Guo, *CrytEngComm*, 2012, **14**, 8342−8344.
11. W. Chen, N. Zhang, M. Y. Zhang, X. T. Zhang, H. Gao and J. Wen, *CrystEngComm*, 2014, **16**, 1201–1206.
12. Z. Q. Liu, W. Y. Huang, Y. M. Zhang, Y. X. Tong. *CrystEngComm*, 2012, **14**, 8261 - 8267.
13. Y. P. Yuan, L. W. Ruan, J. Barber, S. C. J. Loo, C. Xue, *Energy. Environ. Sci*., 2014, **7**, 3934-3951.
14. M. Y. Zhang, C. L. Shao, J. B. Mu, Z. Zhang, Z. C. Guo, P. Zhang, Y. C. Liu, *CrystEngComm*, 2012, **14**, 605-612.
15. M. Y. Zhang, C. L. Shao, Z. C. Guo, J. B. Mu, Z. Y. Zhang, P. Zhang, Y. C. Liu, *ACS Applied Materials & Interfaces*, 2011, **3**, 2573-2578.
16. S.W. Cao, J. Fang, M. M. Shahjamali, F. Y. C. Boey, J. Barber, S. Loo, C. Xue *RSC Adv*., 2012, **2**, 5513-5515 .
17. Y. P. Yuan, L. S. Yin, S. W. Cao, L. N. Gu, G. S. Xu, P. W. Du, H. Chai, Y. S. Liao, C. Xue, *Green Chem*., 2014, **16**, 4663-4668.
18. S. W. Cao, Z. Yin, J. Barber, F. Y. C. Boey, S. C. J. Loo, C. Xue, *ACS Appl. Mater. Interfaces*, 2012, **4**, 418−423.
19. Z. Yi, J. Ye, N. Kikugawa, T. Kako, S. Quyang, H. Stuart Williams, H. Yang, J. Cao, W. Luo, Y. Liu and R. L. Withers, *Nat. Mater.*, 2010, **9**, 559−564.
20. Xiangjiu Guan and Liejin Guo, ACS. Catal. 2014, 4, 3020−3026
21. Y. P. Bi , H. Y. Hu, S. X. Ouyang, Z. B. Jiao, G. Lu, J. H. Ye, *Chem.−Eur. J*. 2012, **18**, 14272−14275.
22. W. Teng, X. Li, Q. Zhao, J. Zhao, A. Zhang, *Appl. Catal. B:Environ.* 2012, **125**, 538−545.
23. X. Yang, J.Qin, Y. Jiang, R. Li, Y. Li, H. Tang, *RSC Adv*. 2014, **4**, 18627−18636
24. Y. P. Bi , H. Y. Hu, Z. B. Jiao, H. C. Yu, G. X. Lu, J. H. Ye, *Phys. Chem. Chem. Phys.*, 2012, **14**, 14486-14488
25. H. Y. Hu,Z. B. Jiao,H. C. Yu,G. X. Lu,J. H. Ye and Y. P. Bi, *J. Mater. Chem. A*, 2013, **1**, 2387-2390
26. C. N. Tang, E. Z. Liu, J. Fan, X. Y. Hu, L. M. Kang, J. Wan, *Ceram. Inter*. 2014, **40**, 15447-15453.
27. H. L. Lin, H. F. Ye, B. Y. Xu, J. Cao, S. F. Chen, *Catal. Commun.* 2013, **37**, 55–59
28. Z. K. Cui, M. M. Si, Z. Zheng, L. W. Mi, W. J. Fa, H. M. Jia, *Catal. Commun.* 2013, 42, 121–124.
29. L. Cai, Q. Y. Long, C. Yin, *Appl. Surf. Sci*. 2014, **319**, 60–67
30. H. C. Yu, Q. S. Dong, Z. B. Jiao, T. Wang, J. T. Ma, G. X. Lu and Yingpu Bi, *J. Mater. Chem. A*, 2014, **2**, 1668-1671
31. P. Wang, B. Huang, X. Qin, X. Zhang, Y. Dai, *Inorg. Chem*. 2009, **48**, 10697−10702.
32. J. W. Xu, Z. D. Gao, K. Han, Y. M. Liu Y. Y. Song, *ACS Appl. Mater. Interfaces*, 2014, **6**, 15122−15131.